

Site Amplification, Q_s , and Source Parameterization in Guwahati Region from Seismic and Geotechnical Analysis

S. K. Nath,¹ A. Raj,¹ J. Sharma,¹ K. K. S. Thingbaijam,¹ A. Kumar,¹ D. R. Nandy,² M. K. Yadav,⁶ S. Dasgupta,³ K. Majumdar,³ J. R. Kayal,³ A. K. Shukla,⁵ S. K. Deb,⁷ J. Pathak,⁸ P. J. Hazarika,⁹ D. K. Paul,¹⁰ and B. K. Bansal⁴

Indian Institute of Technology Kharagpur

INTRODUCTION

As devastating earthquakes continue to inflict widespread destruction to life and property and hinder the development of urban areas, the technical and scientific problems of seismic hazard assessment and risk-related issues warrant urgent attention. In this regard, seismologists play a key role in defining the source parameters of earthquakes and estimating the associated site-specific ground motion amplification commonly termed site response. The relevant analyses are usually performed using either recorded ground motion for a handful of seismic events of moderate to large magnitude or by synthesizing stochastic processes based on the observational data. The hazard projection is aimed at a great earthquake or a maximum earthquake or maximum credible earthquake on probabilistically/deterministically defined terms for a seismic zone under investigation. Seismic sources generally are characterized by well-defined physical parameters such as corner frequency f_c , seismic moment M_0 , and stress drop $\Delta\sigma$, derived directly from waveform data, *i.e.*, strong ground motion records for events with significant magnitude. On the other hand, site amplification of ground motion is attributed to either the geomorphological features that produce scattering, focusing, or defocusing of incident energy or thick alluvium-filled terrain that causes reverberations due to trapped energy. The potentially severe consequences of this

phenomenon have been demonstrated in the damage patterns of several earthquakes, such as the 1985 Michoacan, Mexico, earthquake (Singh *et al.* 1988), the 1988 Armenian earthquake (Borcherdt *et al.* 1989), and the 1989 Loma Prieta earthquake (Hough *et al.* 1990; Borcherdt and Glassmoyer 1992).

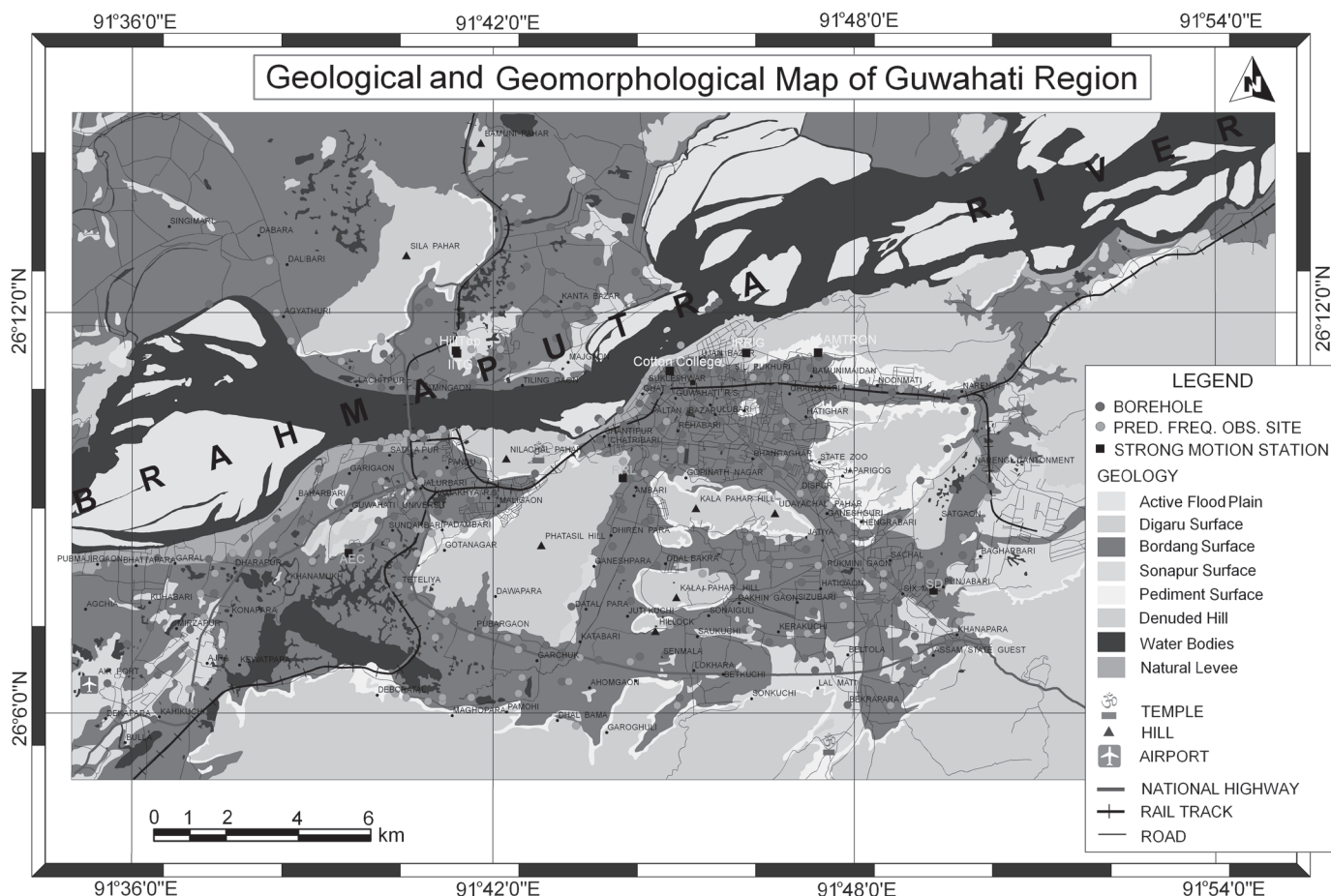
Another aspect of ground motion analysis or synthesis is the attenuation of seismic waves along the propagation path connecting the earthquake source and the recording site (observatory). The attenuation may be attributed to degradation in the elastic properties such as shear and compressional moduli and the scattering of seismic waves caused by heterogeneities in the Earth's interior. The strong-motion attenuation feature as defined by Wu and Aki (1985) is an exponential function of the type $Q_s (= Q_0 f^n)$.

In an attempt to achieve site-specific seismic hazard analysis for the seismogenic northeast Indian city of Guwahati, the capital of the state of Assam, we performed a detailed analysis related to earthquake source, site, and attenuation using available strong ground-motion data of recent earthquakes recorded in the territory. Following Boore (1983), we then undertook a rigorous stochastic synthesis to benchmark the findings.

STUDY REGION

The greater Guwahati region covers an area of approximately 600 km² (longitude 91°30'–91°50'E and latitude 26°05'–26°12'N) and is the gateway of the seven sister states of the northeast Indian Territory, strategically located on the southern bank of the Brahmaputra River. It has been placed in seismic hazard zone V with peak ground acceleration (PGA) > 0.4 g (1 g = 980 gal = 980 cm/s²), the highest seismic hazard level depicted in the seismic hazard zonation map of India (Bureau of Indian Standards 2002). Recently, the city of Guwahati has experienced unprecedented population growth and rapid urbanization. Moreover, owing to the geological

1. Indian Institute of Technology, Kharagpur
2. Formerly with Geological Survey of India
3. Geological Survey of India
4. Seismology Division, Department of Science and Technology
5. India Metrological Department
6. Assam Electronics Development Cooperation Ltd.
7. Indian Institute of Technology Guwahati
8. Jorhat Engineering College
9. Assam Engineering College
10. Indian Institute of Technology Roorkee



▲ **Figure 1.** Geological and geomorphological map of the Guwahati region. The borehole and ambient noise survey locations are indicated by colored dots (in dark red and light green, respectively) while the strong motion recording stations are depicted by black boxes.

and seismotectonic complexities that dominate the region, Guwahati has great earthquake vulnerability. An effort to assess the level of seismic hazard in the region is, therefore, not only important but also imperative.

Geology and Geomorphology

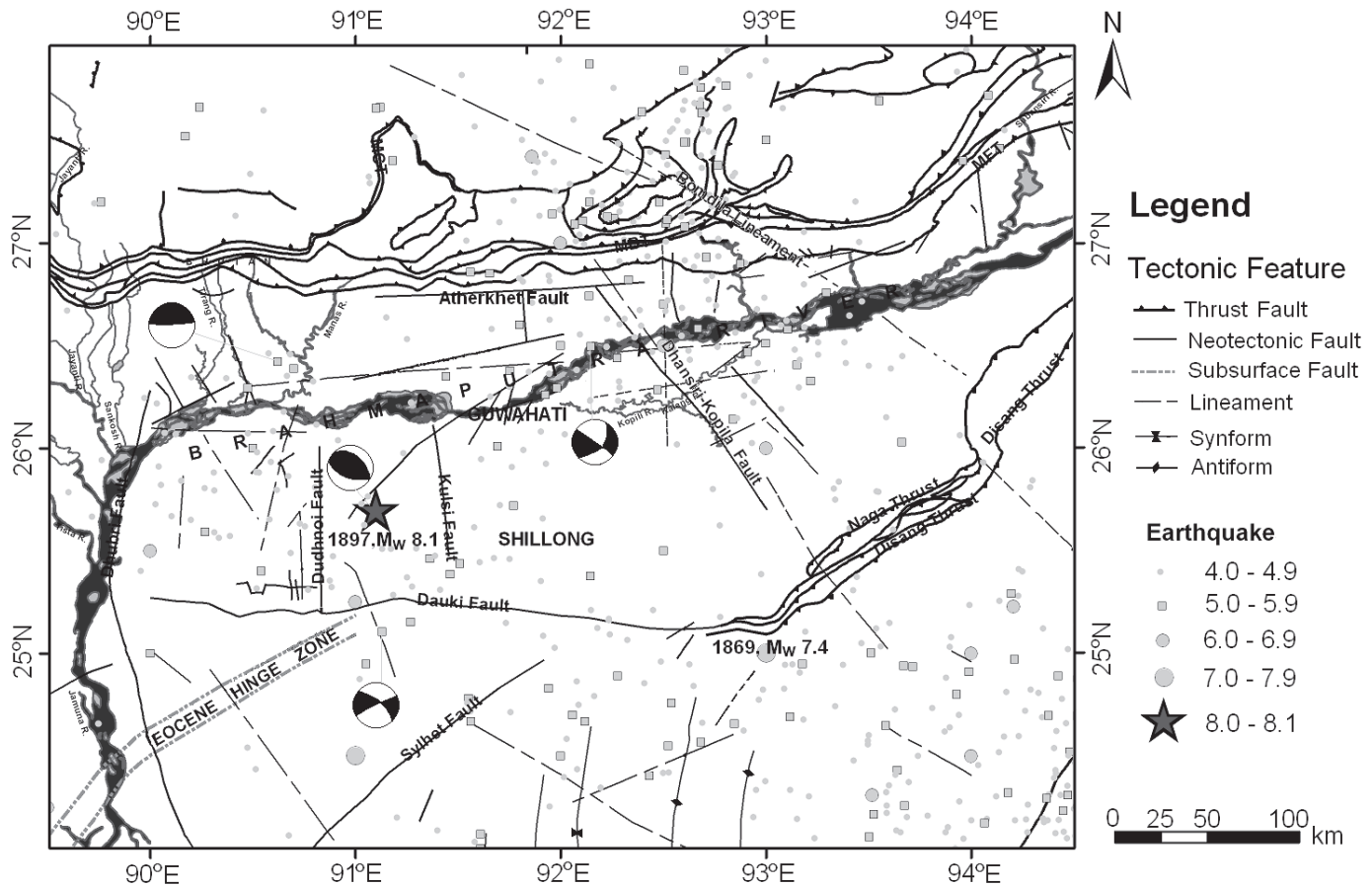
The Guwahati region mainly consists of two types of geological formations: 1) Precambrian granitic rocks that form the hill tracts and isolated hillocks, and 2) Quaternary alluvium found in the valley. The geological and geomorphological map shown in figure 1 is synthesized from Survey of India (SOI) topographic maps with further inputs from IRS PAN and LISS III satellite images in digital format and an extensive GPS-based point survey. According to lithological characteristics, order of superposition, state of weathering, and unconformities, the deposits of the Brahmaputra River have been divided into five units: active flood plain and levee deposit, Digaru surface, Bordang surface, Sonapur surface, and pediment surface.

Important faults in the area include: 1) a NE-SW trending fault cutting across the Dipar beel, which runs for about 15 km along the Chotanagar-Maligaon area; 2) a N10° E-S10°W trending fault running for about 10 km between Kalapahar and Fatasil hills; 3) a N40°E-S40°W trending fault passing along the

Tepar beel, traversing for about 20 km from the southern foothills to the Brahmaputra River; and 4) a fault running almost E-W from near Khanapara westward to the Dipar beel between the southern hills and the isolated hills of Kalapahar and Fatasil (Dasgupta *et al.* 2000). A seismotectonic map covering approximately 200 km around Guwahati is depicted in figure 2.

Seismotectonic Setting

The study region is surrounded on all sides by highly active tectonic blocks: the Himalayan collision zone to the north and the northeast, the Naga thrust region to the east, and the Shillong plateau-Mikir hills tectonic block to the south and southwest. The contemporary tectonics show that active Himalayan frontal thrusts and crosscutting faults have been generating many shallow and small-to-moderate earthquakes (Nandy 2001). On the other side, beyond the Naga thrust zone, active subduction along the Indo-Myanmar mobile belt and the conjugate faults lying across this belt has been producing significant earthquakes that have been felt in the greater Guwahati region. However, strictly speaking, the Guwahati region falls in the domain of the Shillong plateau-Mikir hills block as exhibited by the widespread damage reported for the 1897 Great Shillong earthquake that devastated the region.



▲ **Figure 2.** A seismotectonic map covering approximately 200 km around Guwahati. The tectonic features and the beach balls are modified from Dasgupta *et al.* (2000) while the seismicity is adopted from the M_w consistent homogeneous catalog of Thingbaijam *et al.* (2008) and Thingbaijam and Nath (2008). The beach ball representing the 1897 Great Shillong earthquake is taken from Bilham and England (2001).

DATA

Kinematics Altus K2 strong-motion accelerographs were installed in the Guwahati region by the Indian Institute of Technology (IIT), Guwahati, as a part of a Department of Science and Technology (DST) initiative for seismic microzonation of the region. The dynamic range of the systems is 108 dB, 200 samples/s and 18-bit resolution. Each of the systems has been set with a trigger level of 0.1% of the full-scale sensitivity (2 g). The present analysis is based on five earthquakes that were recorded by the instruments during 2006 with good signal-to-noise ratio (≥ 3). The recording history for the events is listed in table 1.

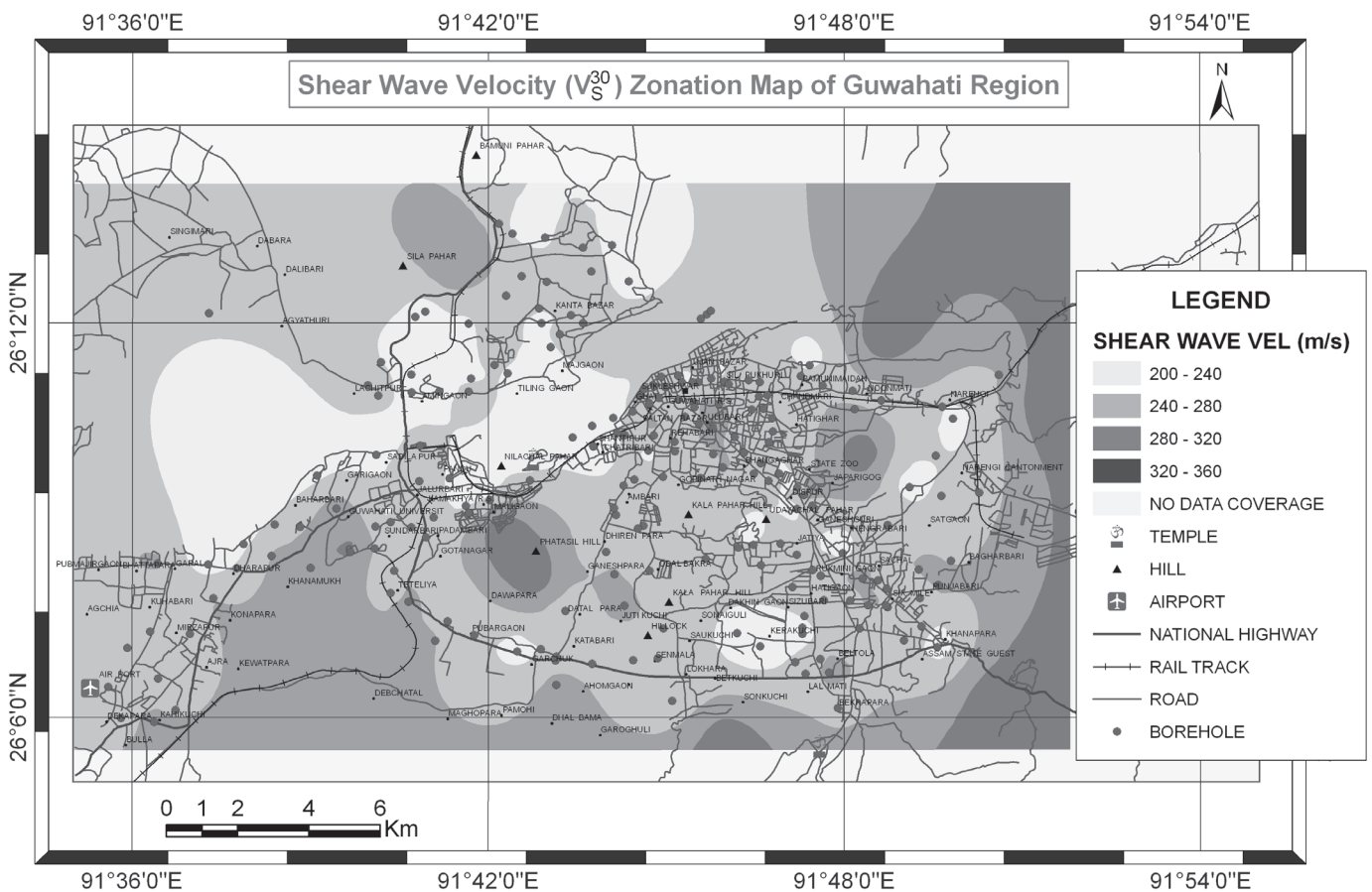
The uncorrected accelerograms, $x(n)$, recorded by a station, were corrected for the system response and baseline adjustments following a standard algorithm incorporated in the software package of M/S Kinematics Inc. The onset of S -wave arrival occasion (t_o) was estimated in $x(n)$. Thereafter, $x(n)$ was bandpass-filtered between 0.1 and 30.0 Hz. A time window of 10-s duration starting from t_o and containing the maximum of the S -wave arrival packet was selected from the filtered dataset, $b(n)$, for the succeeding analysis.

Furthermore, microtremor measurements in the study region were performed jointly by the India Meteorological Department, New Delhi, and the Geological Survey of India, Kolkata, during February–May 2003 by deploying several digital seismic recorders with short-period velocity sensors. Approximately one station per square kilometer was considered, and the observations were carried out at the 141 recording stations shown in figure 1. The exact locations of the stations were determined by the built-in GPS system with a precision of 0.0001 degree. The instruments were installed for a period ranging from one hour to a maximum of 48 hours.

In yet another study, geotechnical data were acquired by Assam Engineering College at 200 borehole locations also depicted in figure 1. At each site, standard penetration test (SPT) data were collected at depths ranging from 6 m to 30 m. Most of these sites are located downtown and along either side of the Guwahati-Shillong road. Depthwise N -value data have been logged for each site, which in turn have been converted to S -wave velocity using empirical relations given by Fumal and Tinsley (1985), Tonouchi *et al.* (1983), and Kayabali (1996) with the lithological constraints. The S -wave velocity distribution map is depicted in figure 3.

TABLE 1
Guwahati Strong Motion Array Recording History for Five Earthquakes

	Event No.				
	1	2	3	4	5
Date (yyyymmdd)	20060214	20060223	20060812	20061106	20061110
Lat. (°N)	27.70	27.20	24.70	24.74	24.60
Lon. (°E)	88.80	92.00	92.75	95.23	92.32
Mag. (m_b)	5.4	5.2	4.9	4.8	4.9
Depth (km)	20.1	33.0	46.2	122.6	43.1
Station					
COTTON (26.187° N, 91.743°E)				✓	✓
HILLTOP (26.193°N, 91.692°E)				✓	
IITG (26.187°N, 91.690°E)		✓	✓	✓	✓
IRRIG (26.184°N, 91.772°E)	✓	✓	✓	✓	
AMTRON (26.185°N, 91.786°E)	✓	✓			✓
AEC (26.141°N, 91.661°E)	✓	✓			
RRL (26.158409°N, 91.735542°E)				✓	
SD (26.132° N, 91.821°E)			✓		
Magnitudes are taken from the U.S. Geological Survey National Earthquake Information Center earthquake catalog.					



▲ **Figure 3.** The shear wave velocity distribution map of the Guwahati region obtained from standard penetration test (SPT) data at 200 borehole locations across the region.

SEISMOLOGICAL ANALYSIS/SYNTHESIS

Following Andrews (1986), Lermo and Chavez-Garcia (1993), and Nath *et al.* (2005), the amplitude spectrum of the i th event recorded at the j th station for the k th frequency $A(r_{ij}, f_k)$ can be written in the frequency domain as a product of a source spectral function $SO_i(f_k)$, a propagation path term $P(r_{ij}, f_k)$, and a site spectral function $SI_j(f_k)$ as follows,

$$A(r_{ij}, f_k) = SO_i(f_k) \times SI_j(f_k) \times P(r_{ij}, f_k). \quad (1)$$

The propagation path term as defined by Hartzell (1992) and Boore (1983) can be expressed as

$$P(r_{ij}, f_k) = G(r_{ij}) e^{\frac{-\pi f_k r_{ij}}{Q_s(f_k) \beta}}, \quad (2)$$

where $G(r_{ij})$ accounts for geometrical spreading and $Q_s(f_k)$ and β are S -wave frequency-dependent quality factor and velocity of the medium, respectively. Average shear velocity on the basis of the crustal velocity model determined for the study region by Mitra *et al.* (2006) corresponds to $\beta = 3.25$ km/s. Further, following Ordaz and Singh (1992), the geometrical spreading can be specified as

$$G(r_{ij}) = \begin{cases} \frac{1}{r_{ij}} & r \leq r_y \text{ km} \\ \frac{1}{\sqrt{r_{ij} r_y}} & r > r_y \text{ km} \end{cases} \quad (3)$$

where r_y is considered twice the thickness of the crustal layer to take into account the possible arrival of surface waves in the windowed data (Herrmann and Kijko 1983). The crustal thickness in the study region varies from 40 km to 50 km, and hence r_y is considered to be within 100 km.

Site Response and Predominant Frequency Estimation

Site response can be estimated through several techniques (Field and Jacob 1995). In the present study, horizontal to vertical spectral ratio (HVSR; Langston 1979; Lermo and Chavez-Garcia 1993; Nath *et al.* 2005) has been employed to evaluate the site amplification factor with respect to a reference site at a separate location IITG. The result has been considered as a representative site-response analysis in the study area. The above method also helps in estimating the fundamental resonant frequency of sediments (Field and Jacob 1995).

The site amplification factor estimated by HVSR $_{ij}(f_k)$ or receiver function technique can be computed at each j th site for the i th event at the central frequency f_k from the root mean square (rms) average of the amplitude spectra,

$$HVSR_{ij}(f_k) = \frac{\frac{1}{\sqrt{2}} \sqrt{absH_{ij}(f_k)|_{NS}^2 + absH_{ij}(f_k)|_{EW}^2}}{absV_{ij}(f_k)}, \quad (4)$$

where $H_{ij}(f_k)|_{NS}$, $H_{ij}(f_k)|_{EW}$, and $V_{ij}(f_k)$ represent Fourier spectra of the NS, EW, and vertical components respectively.

Because of the extensive geotechnical survey coverage of the entire territory, we attempted to correlate the site responses derived from the strong-motion data with those derived from geotechnical considerations. Site response from geotechnical investigation involves a combination of wave propagation theory with the material properties and the expected ground motion computed at the site of interest. Several algorithms are available for seismic response analysis for horizontally layered soil deposits in which recurrent and circular soil behavior can be simulated using a linear equivalent model of a nonlinear phenomenon (Kramer 1996). Generally, an iterative process is used to compute shear modulus and damping compatible with the equivalent uniform strain induced in each sublayer to account for the nonlinear behavior of soil. Each geological unit, *e.g.*, soil profile, is defined by its shear wave velocity, damping, total unit weight, and thickness. The initial estimate of damping is usually taken to be 5% for soil. SHAKE2000 has been used for geotechnical analysis performed in this study.

The frequency at which site amplification shows the highest value is taken as the predominant frequency of the site. It can be estimated through site response analysis using the spectral ratio method from seismic event data. In addition, an ambient noise survey can be also used for this purpose. Several numerical, empirical, and experimental methods for soil characterization and their application in several regions are given by Bard (1995) and Kudo (1995). Experimental methods based on ambient noise data have been found to be the most economical and less time consuming (Nakamura 1989, 1996) when developing a first-cut hazard map based on a predominant frequency distribution that favors recent/new or older alluvium variation. Nakamura proposed an approximate procedure for removing the source effects from micro-tremor records based on a modification of the conventional transfer function of the site considering that a) the horizontal tremor amplifies through multireflection of the S wave, while the vertical tremor amplifies through multireflection of the P wave; and b) the effect of Rayleigh waves appears in the vertical tremor only. Reasonably, the fundamental frequencies of soft deposits could be best estimated by the above approximations. To avoid spurious peaks linked with sharp troughs on the spectrum and for clear identification of peak frequency, spectra are appropriately smoothed by cubic spline interpolation.

Source Parameterization and Quality Factor Q_s

Following Hwang and Huo (1997) and Brune (1970), Brune's omega square model for an earthquake source of the i th event represented by $SO_i(f_k)$ can be defined in the acceleration spectral domain as

$$SO_i(f_k) = \frac{R_{\theta\phi} F(2\pi f_k)^2}{\sqrt{2}(4\pi\rho\beta^3)} \dot{M}_{oi}(f_k), \quad (5)$$

where $R_{\theta\phi}$ ($= 0.63$) is the radiation pattern averaged over an appropriate range of azimuths and take-off angles, F ($= 2.0$) accounts for the amplification of the seismic wave at the free surface, ρ ($= 2.7$ gram/cc) is the average crustal density, β ($= 3.25$ km/s) is the shear wave velocity at the source region, and \dot{M}_{oi} is the moment rate spectrum. The fraction given by $\sqrt{2}^{-1}$ accounts for the partitioning of S -wave energy into two horizontal components and is referred to as partition function. The moment rate spectrum $\dot{M}_{oi}(f_k)$ can be expressed as

$$\dot{M}_{oi}(f_k) = \frac{M_{oi}}{1 + \left(\frac{f_k}{f_{ci}}\right)^{\gamma_i}}, \quad (6)$$

where M_{oi} , f_{ci} , and γ_i , respectively, are the scalar moment, corner frequency, and high frequency spectral fall-off associated with the i th earthquake.

Brune's displacement spectra, defined by equation (7), are iteratively correlated within the frequency range of 0.1 to 20 Hz (the predominant frequency band of strong ground motion response spectra for engineering application) with the corrected transverse component of the observed accelerogram derived from the SH component at all the recording stations until the best possible value of the correlation coefficient is achieved:

$$D(f, r) = \frac{\pi_0 G(r) \exp\left(\frac{-\pi f t}{Q_s}\right)}{\left[1 + \left(\frac{f}{f_c}\right)^\gamma\right]}, \quad (7)$$

where $D(f, r)$ is the displacement spectrum, f is the frequency of interest in Hz, t is the travel time in seconds, $G(r)$ is the geometrical spreading, and r is the source receiver distance in kilometers. The displacement spectra fall-off provides the corner frequency f_{ci} . The initial value of γ_i has been considered equal to 2.0 (Nath *et al.* 2005). π_0 , Q_s , and γ_i have been estimated through simultaneous inversion of displacement spectra. Stress drop $\Delta\sigma$ and seismic moment M_0 have been estimated using equations given by Brune (1970) and Hanks and Kanamori (1979) as

$$M_0 = \frac{4\pi\rho\beta^3\pi_0}{FR_{\theta\phi}} \quad (8)$$

and

$$\Delta\sigma = \frac{0.4397M_0}{r_d^3}, \quad (9)$$

where r_d is defined as radius of rupture such that

$$r_d = \frac{2.34\beta}{2\pi f_c}. \quad (10)$$

Generation of Synthetic Seismogram using Stochastic Method of Simulation

The standard convolution model of equation (1) has been used for the simulation of ground motion. The amplitude spectrum $A(\omega)$ can be written in the frequency domain as the product of source function $SO(\omega, \omega_c)$, propagation path term $P(\omega)$, and a site function $SI(\omega)$ (Lermo and Chavez-Garcia 1993; Nath *et al.* 2005) as

$$A(\omega) = SO(\omega, \omega_c) \times SI(\omega) \times P(\omega). \quad (11)$$

The acceleration spectra often show a sharp decrease with increasing frequency, so a high-cut filter $F(\omega)$ is incorporated in equation (11), converting it to

$$A(\omega) = SO(\omega, \omega_c) \times SI(\omega) \times P(\omega) \times F(\omega). \quad (12)$$

Following Anderson and Hough (1984), the high-cut filter $F(\omega)$ has been assumed to be

$$F(\omega) = e^{-k\omega/2}, \quad (13)$$

where k is a spectral decay parameter and controls the delay rate at higher frequencies.

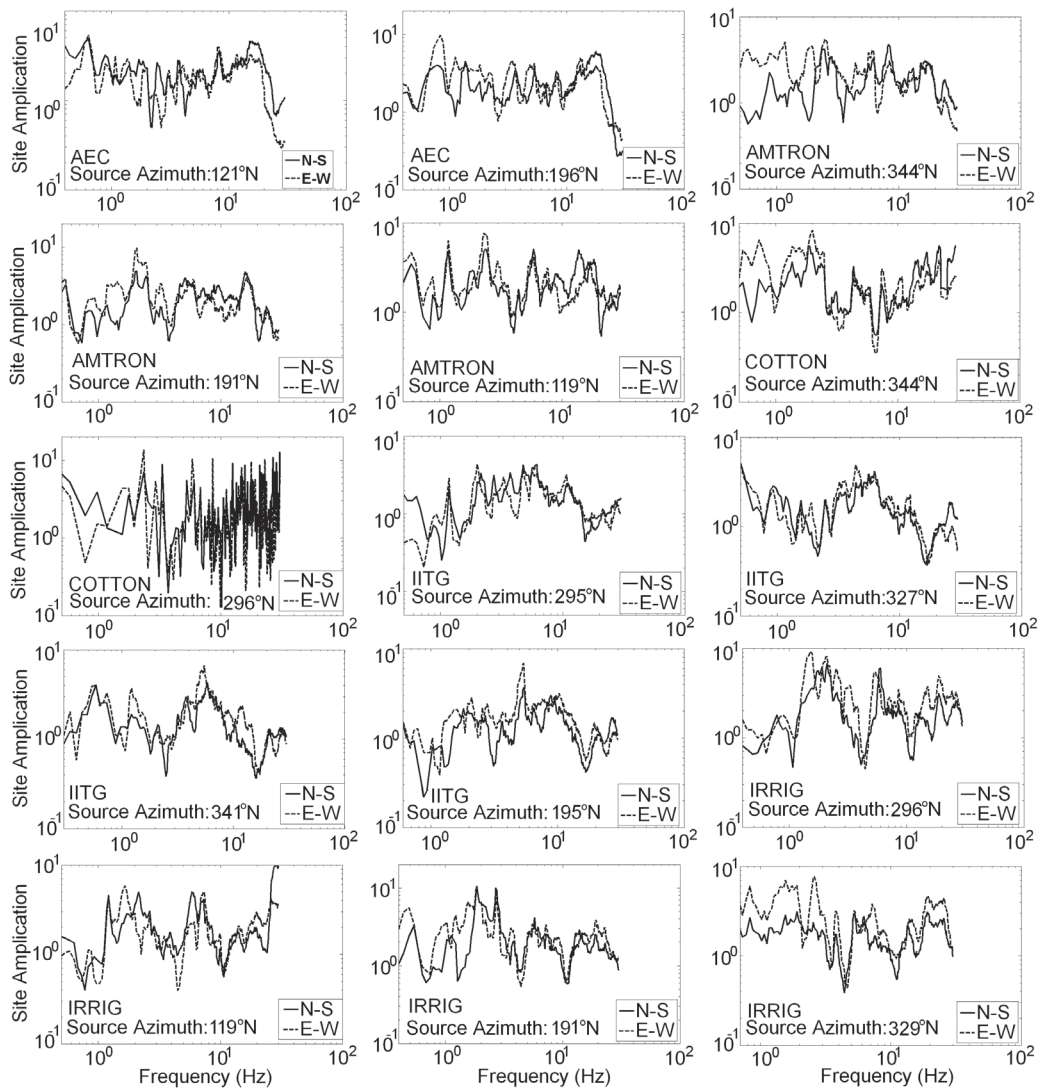
Source function $SO(\omega, \omega_c)$ and propagation path term $P(\omega)$ have been computed via equations 5 and 2 respectively, while HVSR-derived site response has been considered for the site function $SI(\omega)$. To obtain the accelerogram in time domain, first a shaping window is used on Gaussian noise for strong motion duration. Thereafter, the windowed noise is transformed into frequency domain and is normalized. The resultant spectrum is then multiplied by ground motion spectrum and is inverse-transformed to time domain. The ground motion duration is the sum of source duration T_s and the duration of the path. Following Hanks and McGuire (1981), T_s is related to the corner frequency as

$$T_s = f_c^{-1}. \quad (14)$$

The shaping window $\omega(t)$ used to generate an accelerogram in the time domain is given as

$$\omega(t) = at^b e^{-at} H(t), \quad (15)$$

where $H(t)$ is the Heaviside unit -step function. This window represents an averaged envelope of the squared acceleration time series (Saragoni and Hart 1974). The shape parameters b and c are chosen in such a way that the peak of the envelope occurs at some fraction ε of a specified duration T_w , and the amplitude at time T_w is reduced to a fraction η of the maximum amplitude. Thus the following relations are further produced,



▲ **Figure 4.** Representative site response spectra observed at some recording stations.

$$b = \frac{-\varepsilon \ln \eta}{[1 + \varepsilon(\ln \eta - 1)]} \quad (16)$$

and

$$c = \frac{b}{\varepsilon T_w} \quad (17)$$

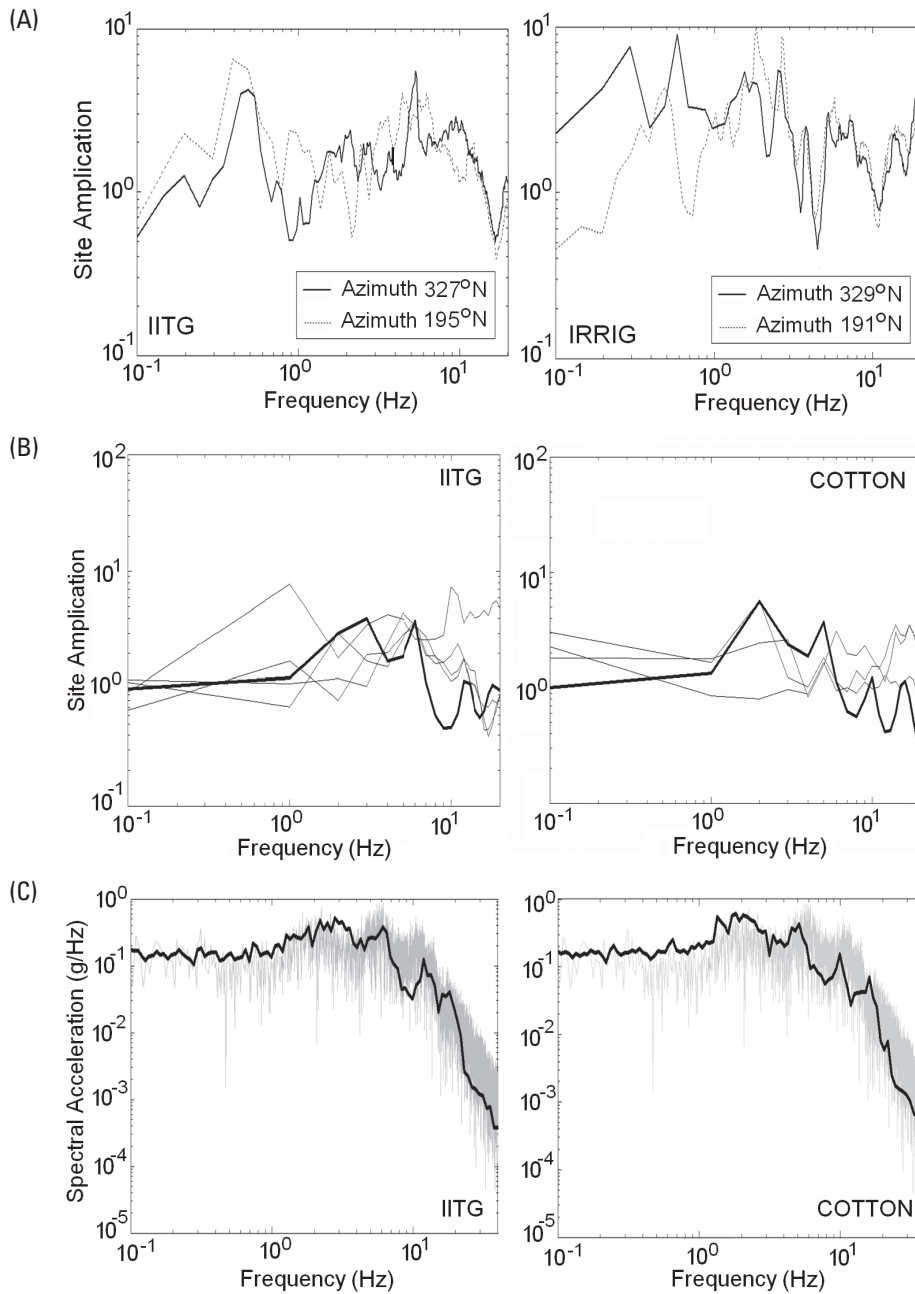
The normalizing factor chosen to give maximum amplitude of unity is given by

$$a = \left(\frac{e}{\varepsilon T_w} \right)^b \quad (18)$$

In the present analysis, η is chosen to be 0.05 and $\varepsilon = 0.2$, consistent with the values of a , b , and c obtained by Saragoni and Hart (1974). The stochastic simulation algorithm of Boore (1983) has been used for this purpose.

RESULTS AND DISCUSSION

Figure 4 depicts the site response computed at the five strong-motion monitoring stations—AEC, AMTRON, COTTON College, IITG, and IRRIG—using recorded events that exhibited varying source azimuths from 119°N to 344°N. Both the NS and EW components of the estimated site response display similar trends with either minor or no variation at all. Therefore, we have been able to compute rms of NS and EW component site amplification for all the events at each station. The representative values at IITG and IRRIG respectively are depicted in figure 5(A). The rms values corresponding to strikingly different azimuths exhibit significant variations as observed for the azimuths of 195°N and 327°N at IITG and 191°N and 329°N at IIRIG. This may be attributed to variations in source radiation pattern, scattering, and diffraction associated with the azimuthal deviations. On the other hand, the site responses estimated through geotechnical and waveform data, respectively, inherently implicate different methodologies. Therefore,



▲ **Figure 5.** (A) Spectral ratio estimate of rms site response at representative stations IITG at source azimuth 195°N and 327°N and IRRIG at source azimuth 191°N and 329°N. (B) Comparison of site amplification estimated by geotechnical analysis (bold line) with HVSR (lighter shade). (C) Comparison of spectral acceleration computed using site amplification derived from geotechnical analysis (bold line) with the acceleration spectra simulated using HVSR site amplification (lighter shade).

a correlation study between the site amplification values derived from the two has been undertaken to establish consistency in the estimated values. Figure 5(B) depicts the variation of site amplification estimated through geotechnical analysis as well as through HVSR. The former corresponds to the boreholes - 146 and 47, which are respectively located in the immediate proximity of stations IITG and COTTON. It has been seen that there is a reasonable agreement between the two different perspectives in the frequency band of 0.1–10.0 Hz. However, the observed stray scatterings indicate that the geotechnical analysis under-

estimates the site response in the higher frequency domain. A similar observation in east-central Iran has been reported by Panah *et al.* (2002). To understand the effect of this variation on the seismicity of the territory, a scenario earthquake of Mw 8.7 with the source characteristics of the 1897 Shillong earthquake (Bilham and England 2001) has been simulated using the EXSIM code of Motazedian and Atkinson (2005). The comparison plots depicted in figure 5(C) emphasize the coherence between the spectral accelerations generated using the site amplifications separately derived from the strong-motion data and the

geotechnical analysis. The spectral acceleration computed using geotechnically derived site response follows a mean trend of the spectral fluctuations. Furthermore, the corresponding peak ground accelerations have comparable values. As such the PGA values estimated through strong ground motion simulation using geotechnical and HVSr site amplifications respectively correspond to 0.56 g and 0.59 g at the IITG site, and 0.44 g and 0.48 g at the COTTON college site. The peak site amplification and predominant frequency estimated through waveform and geotechnical analysis as listed in table 2 show an overall reasonable agreement. The predominant frequencies obtained from the ambient noise survey and strong-motion data are quite close to each other. However, a few deviated values and likely artifacts correspond to the geotechnically derived data.

The site response at site IITG, which is located in the Sonapur surface geological province near a borehole with sediment thickness of 50 m and effective shear wave velocity of 260.4 m/s, exhibits an amplification factor of 4.5 times the ground motion. The geotechnical analysis at borehole 146, in the immediate vicinity of this site, approximates 4.2 times amplification of the ground motion. Furthermore, the predominant frequency at the station computed through microtremor survey, geotechnical analysis, and earthquake recordings corresponds to 3.4 Hz, 4.0 Hz, and 5.0 Hz, respectively. On the other hand, the COTTON college site is located on the Bordang surface, which is characterized by sediment thickness greater than 50 m and effective shear wave velocity of 223 m/s. The strong-motion data analysis at the site indicated a site amplification factor of 6.5 with a predominant frequency of 2.1 Hz. The corresponding geotechnical analysis at borehole 47, near this site, approximates an amplification factor of 5.6 with a predominant frequency of 2 Hz. The predominant frequency of 1.9 Hz has been obtained through a microtremor survey at this location that corresponds well to the differently estimated values.

Figures 6(A) and 6(B) depict the spatial variation of site amplification and predominant frequency, respectively, for the study region, with the amplification factor as high as 15 and as low as 1, while the predominant frequency varies from 0.2 Hz in the geological domain of the active flood plain to 9.5 Hz in the denuded hills. This is a reasonable correlation of high amplification at lower frequency and low amplification at high frequency, as one would expect from an alluvium-filled basin.

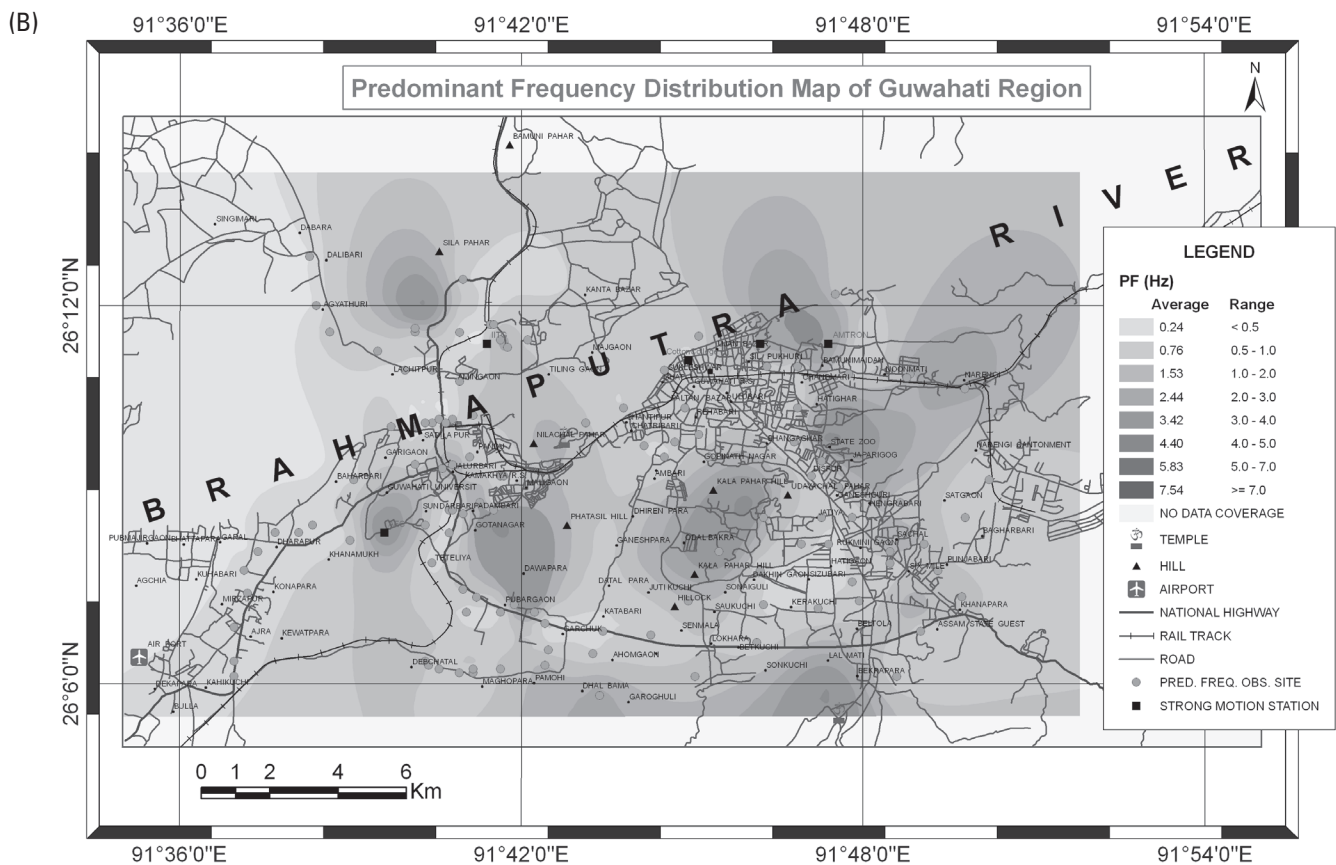
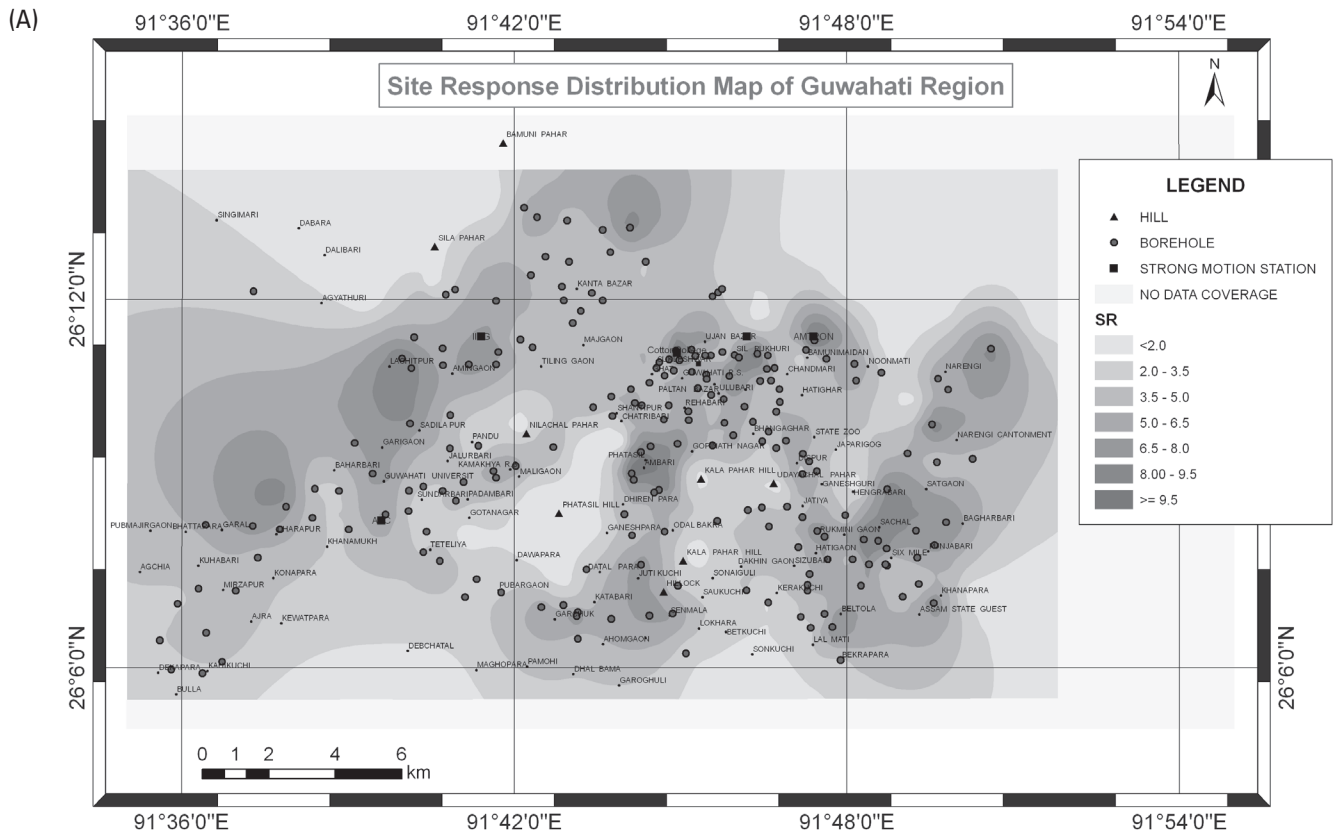
Source and path characterization has been carried out for the five events listed in table 1. Figures 7(A) and 7(B) illustrate the displacement and source spectra for Event No. 3, M_w 4.49, and Event No. 2, M_w 4.84, respectively, at the corresponding recording stations. The displacement and source spectra computed with derived parameters and those corresponding to the observed spectra with the respective correlation coefficients exhibit a reasonable match, as depicted in the two diagrams.

As presented in table 3, the corner frequency f_c varies from 1.0 to 2.1 Hz. The seismic moment M_0 ranges between 1.94×10^{22} and 2.02×10^{23} dyne cm, implicating higher energy concentration for higher magnitude earthquakes, while the stress drop exhibits a range of 49.76 to 442.24 bars. This high value of stress drop implicates a higher radiated seismic energy (Anderson 1997), which indicates a rather severe hazard level in the corresponding fault zone. The shear wave quality factor Q covers a large range of values varying from $180 f^{0.86}$ to $733 f^{0.35}$ with an average of $342 f^{(0.726)}$ in the study region. The variation of path attenuation reveals that lower values of Q are associated with shorter hypocentral distances (100–250 km), while comparatively higher values correspond to larger hypocentral distances (250–400 km). The higher value of Q is likely due to the traveling of seismic waves over larger distances through the deeper crustal layers.

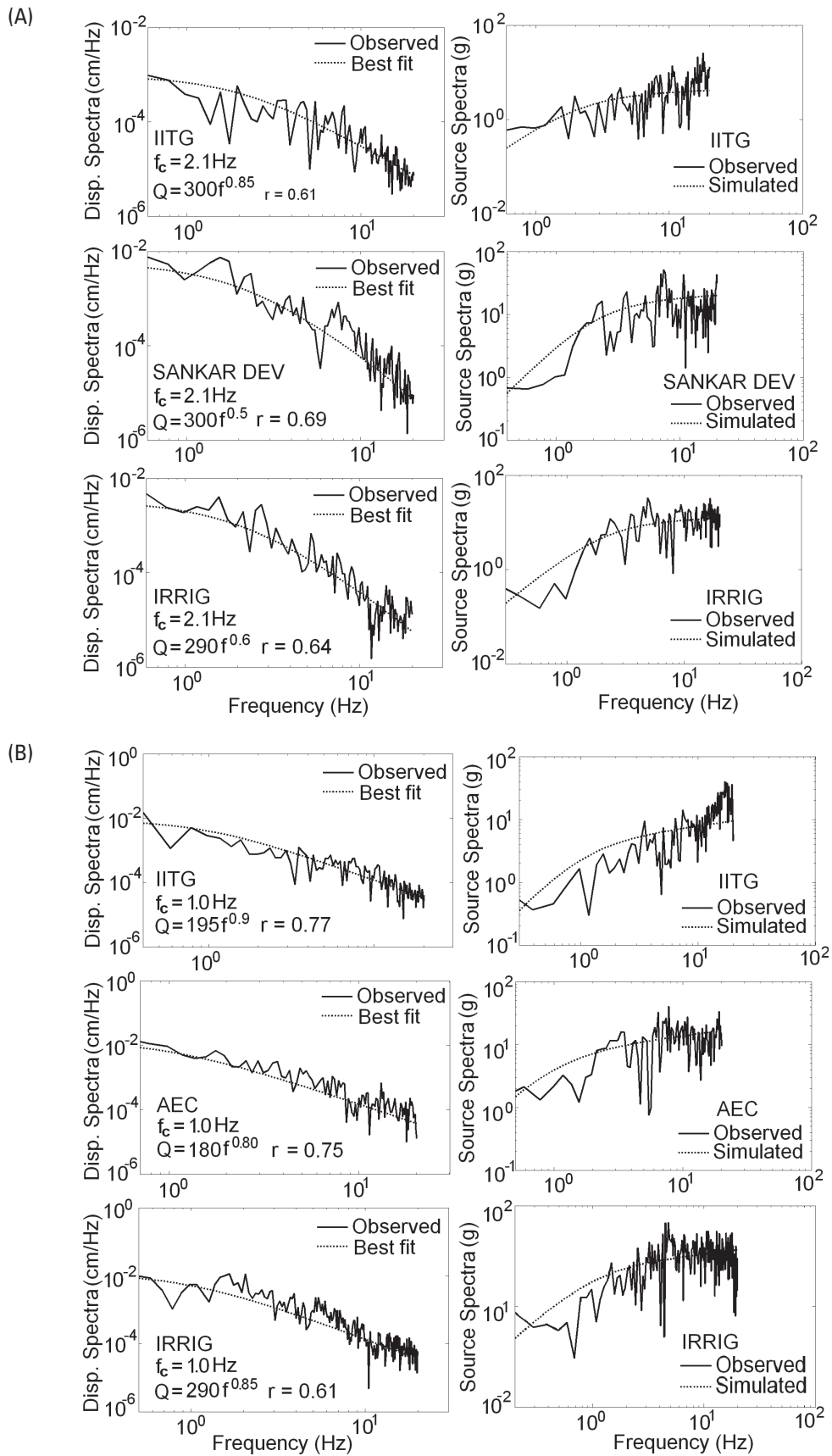
We have made comprehensive efforts to authenticate the computed source, path, and site parameters. A full-scale

TABLE 2
Peak Site Amplification and Predominant Frequency Estimated through Waveform and Geotechnical Analysis

Station	Event No.	Source Azimuth (°N)	PF in Hz			SR at PF	
			Strong Motion	Ambient Noise	Geo-technical	Strong Motion	Geo-technical
COTTON	4	295.50	2.2	1.9	2.0	7.0	5.6
	5	342.40	2.0			6.0	
AMTRON	1	118.90	2.4	1.9	2.0	6.0	3.6
	5	343.60	2.5			5.0	
IITG	2	195.30	5.2	3.4	4.0	5.0	4.2
	3	327.40	4.5			4.0	
	4	295.20	5.0			4.0	
	5	340.90	5.5			5.0	
AEC	1	120.80	0.6	0.7	2.0	4.0	3.7
	2	196.00	0.8			7.0	
IRRIG	1	191.40	2.0	1.9	2.0	10.0	7.2
	2	329.40	2.5			5.5	
	3	295.67	2.0			7.0	



▲ **Figure 6.** (A) Site amplification distribution map obtained through geotechnical analysis at 200 borehole locations. (B) Predominant frequency distribution map of Guwahati region on GIS platform.




▲ **Figure 7.** Displacement spectra and source spectra for (A) Event No. 3 (table 1) and (B) Event No. 2 (table 1) at respective recording stations.

TABLE 3
Estimated value of source parameters – Seismic Moment (M_0), Stress drop ($\Delta\sigma$), Corner Frequency (f_c), and Spectral decay factor (γ). Quality factor Q_s is also listed.

Event No.	M_w	M_0 (dyne-cm)	$\Delta\sigma$ (bars)	f_c (Hz)	γ	$Q_s = Q_0^* f^n$
1	4.82±0.02	(1.94 ±0.18) × 10 ²³	442.24 ±22.4	2.1 ±0.1	2.4 ±0.1	(733±133) $f^{0.35±0.05}$
2	4.84±0.11	(2.02±0.57) × 10 ²³	49.76 ±14.1	1.0 ±0.1	1.75 ±0.1	(180±15) $f^{0.86 ±0.06}$
3	4.49±0.09	(6.05 ±1.31) × 10 ²²	138.32 ±31.0	2.1 ±0.1	1.9 ±0.1	(282±18) $f^{0.7±0.15}$
4	4.57±0.09	(8.06±2.52) × 10 ²²	116.00 ±36.2	1.8 ±0.1	2.1 ±0.1	(452±82) $f^{0.85 ±0.05}$
5	4.53±0.10	(6.92±1.59) × 10 ²²	160.84 ±34.1	2.1±0.1	1.9 ±0.1	(272±28) $f^{0.74 ±0.09}$

M_w values obtained from Hanks and Kanamori (1979)

strong ground motion synthesis has been accomplished at all the recording stations for the entire source azimuthal range and the source radiation patterns through the stochastic algorithm. A few representative accelerograms exhibiting comparisons between the simulated and observed ones in both time and frequency domains are presented in figure 8(A) for Event No. 5, M_w 4.53 (table 1) with stress drop (= 160.84 bars), f_c (= 2.1 Hz), γ (= 1.9), and Q_s (= 272 $f^{0.74}$), and in figure 8(B) for Event No. 3, M_w 4.49 (table 1) for stress drop (= 138.32 bars), f_c (= 2.1 Hz), γ (= 1.9), and Q_s (= 282 $f^{0.7}$). It is evident from these diagrams that the simulated and the observed spectral accelerations are virtually mimicking each other in the frequency band 1 Hz to 10 Hz, the desired frequency bandwidth for the geotechnical/earthquake engineering applications, which is marked with arrows in the respective diagrams. The spectral fall-off at the higher frequency cutoff region can be attributed to the minor deviation observed in the spectral presentations in figures 8(A) and 8(B). However, the time history of the accelerogram has been presented as a mere indicator of comparable seismic event arrivals, not for point comparisons that have been restricted to spectral domain. Table 3 has been updated with the uncertainties computed with ± 1 standard deviation that have been observed to be practically within tolerance limits. These uncertainties could be attributed to simplified mathematical principles/relations used for simulating the otherwise inhomogeneous and anisotropic Earth. 

CONCLUSION

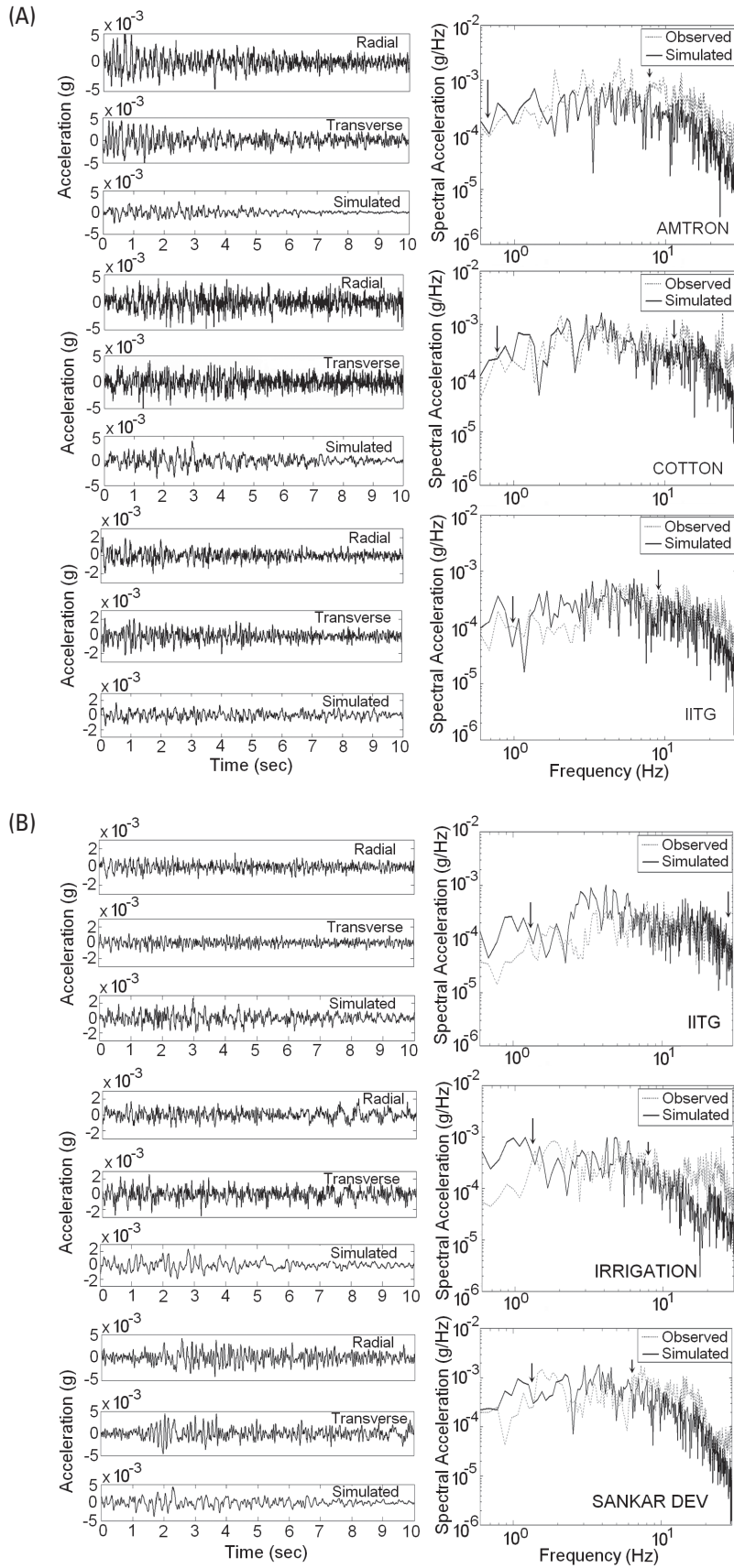
Hybrid seismogeotechnical synthesis uses a moderate-magnitude earthquake recording with complementary geotechnical and ambient noise survey results as a hazard analysis package to generate a seismic hazard scenario for an historical or predicted maximum earthquake. The great earthquakes of 1897 Shillong and 1950 Assam establish a significant threat scenario, to present-day Guwahati city. The hazard scenario in each case can be simulated using the site amplification presented here, either from strong ground motion or geotechnical analysis, to achieve design PGA and response spectra. To this effect, the work reported here presents a benchmark and starting point for future work.

ACKNOWLEDGMENTS

We are grateful to Dr. Susan Bilek, Dr. Chris Cramer, and Dr. Luciana Astiz for their comments and critical suggestions. This research was supported by the Seismology Division, Department of Science and Technology, Government of India vide DST/Exp Group/ Guwahati microzonation/ 2002.

REFERENCES

- Anderson, J. G. (1997). Seismic energy and stress-drop parameters for a composite source model. *Bulletin of the Seismological Society of America* 87 (5), 85–96.
- Anderson, J. G., and S. E. Hough (1984). A model for the shape of the Fourier amplitude spectrum of acceleration at high frequencies. *Bulletin of the Seismological Society of America* 74 (5), 1,969–1,993.
- Andrews, D. J. (1986). Objective determination of source parameters and similarity of earthquakes of different size. In *Earthquake Source Mechanics*, ed. S. Das, J. Boatwright, and C. H. Scholz, 259–268. Washington, DC: American Geophysical Union.
- Bard, P. Y. (1995). Effects of surface geology on ground motion: Recent results and remaining issues. In *Proceedings of the 10th European Conference on Earthquake Engineering*, ed. G. Duma, 305–323. Rotterdam.
- Bilham, R., and P. England (2001). Plateau “pop-up” in the great 1897 Assam earthquake. *Nature* 410, 806–809.
- Bureau of Indian Standards (2002). IS 1893–2002: Indian Standard Criteria for Earthquake Resistant Design of Structures, Part 1—Resistant Provisions and Buildings. New Delhi: Bureau of Indian Standards.
- Boore, D. M. (1983). Stochastic simulation of high-frequency ground motions based on seismological models of the radiated spectra. *Bulletin of the Seismological Society of America* 73 (6), 1,865–1,894.
- Borcherdt, R. D., and G. Glassmoyer (1992). On the characteristics of local geology and their influence on ground motions generated by the Loma Prieta earthquake in the San Francisco Bay region, California. *Bulletin of the Seismological Society of America* 82, 603–641.
- Borcherdt, R. D., G. Glassmoyer, A. Der Kiureghian, and E. Cranswick (1989). *Results and Data from Seismologic and Geologic Studies Following Earthquakes of December 7, 1988 near Spitak, Armenia*, S.S.R. USGS Open-File Report, 89–163.
- Brune, J. N. (1970). Tectonic stress and the spectra of seismic shear waves from earthquakes. *Journal of Geophysical Research* 75, 4,997–5,009.
- Dasgupta, S., P. Pande, D. Ganguly, Z. Iqbal, K. Sanyal, N.V. Venaktraman, S. Dasgupta, B. Sural, L. Harendranath, K. Mazumadar, S. Sanyal, A. Roy, L. K. Das, P. S. Misra, and H. Gupta (2000). *Seismotectonic Atlas of India and Its Environs*. Calcutta: Geological Survey, India.



▲ **Figure 8.** The observed and simulated accelerograms both in time and frequency domain for (A) Event No. 5 (table 1) and (B) Event No. 3 (table 1).

- Field, E. H., and K. H. Jacob (1995). A comparison and test of various site response estimation techniques, including three that are not reference site dependent. *Bulletin of the Seismological Society of America* **85**, 1,127–1,143.
- Fumal, T. E., and J. C. Tinsley (1985). Mapping shear-wave velocities of near-surface geologic materials: Evaluating earthquake hazards in the Los Angeles region—An earth-science perspective, ed. J. I. Ziony. USGS Professional Paper 1360, 127–149.
- Hanks, T. C., and R. K. McGuire (1981). Character of high frequency ground motion. *Bulletin of the Seismological Society of America* **71**, 2,071–2,095.
- Hanks, T. C., and H. Kanamori (1979). A moment magnitude scale. *Journal of Geophysical Research* **84**, 2,348–2,350.
- Hartzell, S. H. (1992). Site response estimation from earthquake data. *Bulletin of the Seismological Society of America* **82**, 2,308–2,327.
- Herrmann, R. B., and A. Kijko (1983). Modeling some empirical vertical component Lg relations. *Bulletin of the Seismological Society of America* **75**, 157–171.
- Hough, S. E., R. D. Borcherdt, P. A. Friberg, R. Busby, E. Field, and K. H. Jacob (1990). The role of sediment-induced amplification in the collapse of the Nimitz freeway during the October 17, 1989 Loma Prieta earthquake. *Nature* **344**, 853–855.
- Hwang, H. H. M., and J. R. Huo (1997). Attenuation relations of ground motion for rock and soil sites in Eastern United States. *Soil Dynamics and Earthquake Engineering* **16**, 363–372.
- Kayabali, K. (1996). Soil liquefaction evaluation using shear wave velocity. *Engineering Geology* **44**, 121–127.
- Kramer, S. L. (1996). Geotechnical earthquake engineering. In *Prentice-Hall International Series in Civil Engineering and Engineering Mechanics*, ed. C. H. Dowding, 255–273. Upper Saddle River, NJ: Prentice-Hall.
- Kudo, K. (1995). Practical estimates of site response. State-of-the-art report, Proceedings of the Fifth International Conference on Seismic Zonation. Nice, France, 1,878–1,907.
- Langston, C. A. (1979). Structure under Mount Rainier, Washington, inferred from teleseismic body waves. *Journal of Geophysical Research* **84**, 4,749–4,762.
- Lermo, J., and F. J. Chavez-Garcia (1993). Site effect evaluation using spectral ratios with only one station. *Bulletin of the Seismological Society of America* **83**, 1,574–1,594.
- Mitra, S., K. Priestley, V. K. Gaur, S. S. Rai, and J. Haines (2006). Variation of Rayleigh wave group velocity dispersion and seismic heterogeneity of the Indian crust and uppermost mantle. *Geophysical Journal International* **164**, 88–98.
- Motazedian, D., and G. M. Atkinson (2005). Stochastic finite-fault modeling based on a dynamic corner frequency. *Bulletin of the Seismological Society of America* **95**, 995–1010.
- Nakamura, Y. (1989). A method for dynamic characteristics estimations of subsurface using microtremors on the ground surface. *Quarterly Report of the Railway Technical Research Institute* **30**, 25–33.
- Nakamura, Y. (1996). Real-time information systems for seismic hazard mitigation UREDAS, HERAS and PIC. *Quarterly Report of the Railway Technical Research Institute* **37** (3), 112–127.
- Nandy, D. R. (2001). *Geodynamics of North Eastern India and the Adjoining Regions*. Kolkata, India: ACB Publications.
- Nath, S. K., V. Madhav, I. Pal, and P. Sengupta (2005). A seismic hazard scenario in the Sikkim Himalaya from seismotectonics, spectral amplification, source parameterization, and spectral attenuation laws using strong motion seismometry. *Journal of Geophysical Research* **110**, B01301, doi: 10.1029/2004JB003199.
- Ordaz, M., and S. K. Singh (1992). Source spectra attenuation of seismic waves from Mexican earthquakes and evidence of amplification in the hill zone of Mexico City. *Bulletin of the Seismological Society of America* **82**, 24–43.
- Panah, A. K., N. H. Moghaddas, M. R. Ghayamghamian, M. Motosaka, M. K. Jafari, and A. Uromieh (2002). Site effects classification in East-Central of Iran. *Journal of Seismology and Earthquake Engineering* **4** (1), 37–46.
- Saragoni, G. R. and G. C. Hart (1974). Simulation of artificial earthquakes. *Earthquake Engineering and Structural Dynamics* **2**, 249–267.
- Singh, S. K., E. Mena, and R. Castro (1988). Some aspects of source characteristics of the 19 September 1985 Michoacan earthquake and ground motion amplification in and near Mexico City from strong motion data. *Bulletin of the Seismological Society of America* **78**, 451–477.
- Thingbaijam, K. K. S., and S. K. Nath (2008). Estimation of maximum earthquakes in northeast India region. *Pure and Applied Geophysics* **165**, 1–13.
- Thingbaijam, K. K. S., S. K. Nath, A. Yadav, A. Raj, Y. M. Walling, and W. K. Mohanty (2008). Recent seismicity in northeast India and its adjoining region. *Journal of Seismology* **12**, 107–123.
- Tonouchi, K., T. Sakayama, and T. Imai (1983). S wave velocity in the ground and the damping factor. *Bulletin of the International Association of Engineering Geologists* **26–27**, 327–333.
- Wu, R. S., and K. Aki (1985). Elastic wave scattering by a random medium and the small scale inhomogeneities in the lithosphere. *Journal of Geophysical Research* **90**, 10,261–10,273.

Indian Institute of Technology
Kharagpur 721302
West Bengal, India
nath@gg.iitkgp.ernet.in
(S.K.N.)